Renewable Energy 36 (2011) 1685–1692

Contents lists available at ScienceDirect

Renewable Energy

journal homepage: www.elsevier.com/locate/renene

An application of the Fast Fourier Transform to the short-term prediction of sea wave behaviour

J. Ross Halliday [a], David G. Dorrell [b,*], Alan R. Wood [c]

[a] Natural Power Consultants Ltd., Dalry, Castle Douglas, Scotland, UK
[b] University of Technology Sydney, School of Electrical, Mechanical and Mechatronic Systems, Sydney NSW 2007, Australia
[c] University of Canterbury, Department of Electrical and Computer Engineering, Christchurch, New Zealand

ARTICLE INFO

Article history:
Received 3 February 2010
Accepted 29 November 2010
Available online 12 January 2011

Keywords:
Fourier transform
Wave prediction
Dispersion relationship
Non-harmonic modelling

ABSTRACT

This paper examines the appropriateness of the Fast Fourier Transform for decomposition and reconstruction of wave records taken at fixed locations and transposed to a different temporal and spatial point. In marine renewable energy, advanced control methods based on the future prediction of waves are being developed. These methods are based on the assumption that a forward looking prediction is available and over the years there has been a conjecture that the FFT may perform this role and that the prediction of wave behaviour at any point on the sea surface should be realizable. The validity of this statement is tested using numerical wave records.

1. Introduction

There are several aspects to the assessment of sea waves in terms of their spectral content and energy resource. Most studies are concerned with resource estimation, particularly in specific locations where the wave energy extraction potential is being considered [1–4]. Some studies address the impact of wave energy generation on the environment [5] and wave energy generation in nearshore locations where the wave spectrum is more chaotic [6]. Wave motion is often studied in relation to the operation of specific energy converters [7,8]. However one issue that is deemed to be useful in the deployment of sea wave energy generators is short term wave prediction using wave measurement devices or predictors at a distance from the generator. This would allow systems to foretell what wave conditions are oncoming so that a time-lag in system reaction can be removed. Essentially it can be tuned. There are many systems in development, examples are shown in Ref [9–11] and these may be aided in their operation by knowledge of the oncoming wave spectrum.

A general misconception in early stage wave energy projects is that this prediction of surface elevation is a trivial problem. This perception is underpinned by observing shoreline waves, which appear to roll onshore with a semi-regular period, reinforcing the image of a theoretical wave of a single fixed frequency. This simplified model lends itself well to exploring the potential that the Fast Fourier Transform (FFT) holds in predicting wave behaviour. However, when taking visual observations to an offshore location it becomes very difficult to track a constant wave crest since the wave groups consist of waves with varying heights and wavelengths; hence, the ideal single-frequency wave model then breaks down. This is further complicated by presence of new and old sea states persisting from multiple directions.

Over the past few decades there have been several studies into the use of the FFT for short term wave prediction. This paper, which expands an earlier paper [12], seeks to gather, implement and build upon outcomes from previous studies in order to develop and examine the point at which the FFT based prediction breaks down. We will go further and attempt to explain why this breakdown occurs.

1.1. Literature review

Short term deterministic prediction of sea waves has been recently studied [13,14]. In the developing wave energy industry, a short term prediction would advantageous in advanced control strategies for various wave devices. These control techniques were briefly reviewed in Ref [15] and would allow economic system utilization. Belmont et al. [16] showed that a prediction of the order of 30 s ahead should be possible. In producing the prediction results it would appear that a limited number of widely spaced wave vectors were used in constructing the source records. The reduced complexity of the input data used should cast some doubt over the validity of the 30-seconds-ahead claim. Zhang et al. [17] went

* Corresponding author.
E-mail address: ddorrell@eng.uts.edu.au (D.G. Dorrell).

0960-1481/$ – see front matter © 2010 Elsevier Ltd. All rights reserved.
doi:10.1016/j.renene.2010.11.035

further in their prediction method by using real directional data and developing a directional hybrid wave model (DHWM) to produce an accurate prediction from a reference sensor to a point a few tens of meters away. In this paper there was limited reference as to whether this prediction was carried out in the time domain.

There have been further prediction-over-distance studies. Refs. [18] and [19] conducted studies with a view to comparing linear and non-linear reconstruction and reported good prediction matches of 70 m and 15 m ahead using omni-directional wave spectra in both small linear wave fields and larger non-linear fields. Ref. [20] showed good prediction over distances to 12 m in a wave-tank with a spectrum of up to 5 frequencies (ranging from 0.67 Hz to 1.67 Hz), but at spectral densities greater than this the predictions began to diverge from the target.

Alternate methods to the FFT have been considered in other fields and brought to bear on the complex problem of time series prediction. At the present, time-series prediction based on neural network processing and genetic algorithms are being developed [21] and methods exist for using alternative transforms and data processing methods such as the Kalman filter [22] or the Hilber-Huang transform [23]. These alternate methods are not explored in this paper.

In examining and recording time series data the Fast Fourier Transform (FFT) is used routinely and a prediction made using this technique would seem to offer a readily accessible option. The available literature has made initial steps towards this goal, however each study has shown initial success with application to more simple problems, but they appear to break down with increasing complexity. This apparent breakdown in the predictions and subsequent explanation was not thought by the authors to have provided sufficient proof in dismissing the FFT as a suitable method on which to base short term prediction algorithms. This paper will attempt to demonstrate the complexity of using such a method in both the time and space domain and will explore the relationship between discrete representation and the dispersal relationship of waves.

1.2. Basic aspects of experimental wave measurement and recent wave generation regional interests

As background, this section outlines some basic wave measurement arrangements (that assume that short term prediction is possible) and recent interest in wave energy generation to illustrate the growing interest in practical generator deployment.

There are many aspects to short term wave prediction in addition to the need for predictive methods. Here, we will review some basic concepts before describing the main work of predictive wave methods in this paper. Because waves are directional, then usually at least two wave measurement devices are needed as illustrated in Fig. 1(a). However, because the spectra, both frequency and direction, is complex and continually changing, it is suggested that an array may be used as shown in Fig. 1(b). However, when using buoys to measure the waves, these tend to drift with the water particle motion and give imprecise spatial measurement; this is illustrated in Fig. 1(c). If the buoy has high precision knowledge of this motion, it is may be possible to account and adjust for the position of the buoy on the wave cycle. For simplicity, and to illustrate the issues with using Fourier series for short-term wave prediction, unidirectional waves are assumed in this paper. The addition of directional variation will further complicate and add errors to the work set out below.

In terms of an overall wave energy generation system context, short term sea wave prediction will continue to be demanded. There are many locations where wave energy systems are being assessed and considered; these include diverse locations such as Hawaii [24, 25], Iran [26], North Atlantic [27, 28] and Alaska [29]. Indeed, the level of study is increasing and it may be possible to combine with offshore wind systems as described in [30] so that combined wave and wind prediction will be advantageous. Larger sea wave systems continue to be studied and developed [31].

2. Wave devices and measurement

In order for prediction techniques to be realizable a method of measurement must be in place in order to accurately record the surface elevation (wave height) at a fixed location. The most cost effective method is to utilize a directional wave measurement buoy moored at a distance from a wave energy device so that reflections are avoided. Other measurement techniques may be considered. For example, satellite or airborne measurement would provide a fixed measurement of the sea surface, but would be prohibitively expensive. A LIDAR (Light Detection and Ranging) device [32] can also provide a fixed measurement but it needs to be mounted at a sufficient elevation above the maximum wave height in order to avoid wave shadowing effects. Wave devices which can survive North Atlantic sea conditions will require a streamlined profile with no elevated structure onto which this type of device can be mounted. However a LIDAR system may be suitable for large-scale device farms with suitable superstructures. A recently developed alternative is to utilize wave data measured by an Acoustic Doppler Current Profiler (ADCP) [33] but this may be limited to shallower water applications.

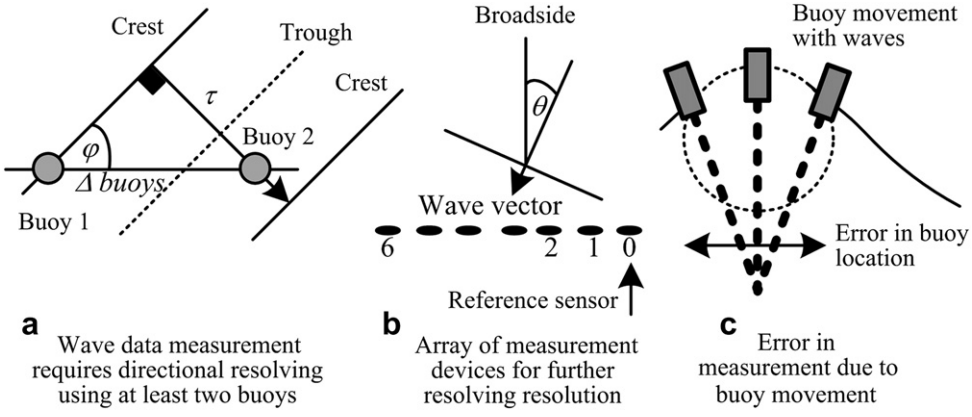

Fig. 1. Aspects of practical wave measurement.

The directional wave buoy will not provide a fixed reference point due to its motion with passing waves and reaction against its mooring. These errors in buoy measurement were described in [34] but may be corrected through signal processing of high precision onboard accelerometer data. The introduction of GPS-based measurement buoys [35] may allow for accurate tracking of the point at which a record is being taken and assist in reconstruction of a fixed point record. For this study it will be assumed that a record of surface elevation for a fixed point on the sea surface is realizable and available.

At the time of this study, real wave records were unavailable; however, the data collected during the WADIC (Wave Direction Measurement Calibration Project) experiment [36], where many records were taken in close proximity, or even other data sources [37], would be ideal for this type of study. The data presently being collected by the University of Exeter at the Wavehub site in Cornwall will be invaluable to future studies of this type. In the absence of real time series, simulated records were created using a method described by Tucker [34] and Dean and Dalrymple [38]. The methodology used in this paper is given in the appendix of [12] where it was modified to remove any harmonic trends in the records.

3. Prediction in time

One of the first steps in analyzing a time series of length T seconds is to take the Fourier transform. As a first step it may be assumed that this method can be used to extend any time series infinitely beyond the length of the original record. As per standard theory the Fast Fourier Transform (FFT) resolves a time series $f(\Delta t \rightarrow T)$ into a summation of harmonically-related sinusoids with unique amplitudes F_n and phases ϕ_n. In a simple prediction application this series of sinusoids may be used with a basic omni-directional linear wave equation for dispersive gravity waves to recalculate the summation of sinusoids at an arbitrary time greater than T s. To achieve this reconstruction we can use the common equation for a Fourier spectrum of waves with magnitude, frequency and phase:

$$\xi(x,t) = \sum_{n=1}^{N} F_n \cos(k_n x - \omega_n t - \phi_n) \quad (1)$$

where F_n is the amplitude of the sinusoid, k_n is the wave number, ϕ_n is the phase of the sinusoid and

$$\omega_n^2 = g k_n \tanh(k_n h)$$

is the dispersal relationship.

3.1. Simulation

The following simulation was set up to demonstrate an ahead-in-time prediction made from the same spatial point at which the source time series was taken. A wave record of length 2400 s was simulated for an 18.6 m/s Pierson-Moskowitz spectrum from 0 to 0.5 Hz using the non-harmonic method as described in the Appendix of [12]. A 18.6 m/s wind (gale force 7) was chosen to allow for ease of characteristic identification in the time series. This wind speed represents poor winter sea conditions off of the west coast of Scotland. It is under these conditions that a potential device would be working at its structural and generating maximums. In worse conditions than these the production would stop and a survival state is implemented [39].

The two controlling variables of the FFT need to be first of all examined. These are T, the length in seconds of the time series; and N, the number of time samples into which the series is split or by Nyquist half the maximum number of frequency values into which the spectrum is resolved. The reciprocal of T governs the lowest frequency/longest wavelength that can be detected. It also controls the frequency resolution where $\Delta f = 1/T$. Table 1 gives various values of T and a suggested minimum number of samples N. The corresponding frequency resolution and the wavelengths of the frequency components around a nominal wavelength of 500 m are displayed. For example with a Δf of 0.00333 Hz the three wavelength components closest to 500 m are 624.5 m, 548.9 m and 486.2 m, an approximate $\Delta\lambda$ of 60–80 m.

The length of T has an important effect on the resolution of the FFT. For longer wavelengths the resolution becomes increasingly worse; for shorter wavelengths the resolution improves.

The controlling parameter N and the number of samples in the record are used to establish the highest frequency which can be recognized before aliasing occurs. This frequency is $N/2T$. Table 1 gives the minimum values for N for an upper detectable frequency limit of 0.5 Hz. Records containing frequencies above this cut-off need to be filtered. Standard wave measurement buoys naturally lose resolution above 0.5 Hz and implement the low-pass filtering onboard [34].

A model was developed which produced a record of 8192 samples over 2400 s. This record was spilt into two halves, the first 1200 s was the reference time series and the second 1200 s is the target series to be predicted. This gave an effective T of 1200 s, N of 4096 samples and $\Delta\lambda$ of 8–16 m. An FFT was then applied to the reference record and the real and imaginary components were retained. A window was not applied to the reference time series as this induces phase shifting. From the data, a wave vector file was generated using the real and imaginary components and this gave the amplitude and phase values for each harmonically-related wave vector. This vector file was then used with (1) to produce a predicted wave record for the time period 1200 s–2400 s which was then compared to the target record.

3.2. Results and interim discussion

Fig. 2 shows the results of the simulation. The upper graph presents the prediction compared to the original reference series for $t = 1200 \rightarrow 1500$ s. The time period and significant wave height show some reasonable agreement but the phasing does not match. The lower graph shows the first 300 s of the original reference record and the first 300 s of the predicted series. They match well. The explanation for this behaviour lies with the FFT itself which is designed to work with periodic time series, e.g.:

$$f(-T \rightarrow 0) = f(0 \rightarrow T) = f(T \rightarrow 2T)$$

If the record from $t = \Delta t \rightarrow T$ is examined the wave vectors returned will exactly represent this series. Recalculating at any other time period will simply be a reproduction of a section of this original time series. Since real waves are known not to display this type of periodicity then the Fourier method does not appear

Table 1
Resolution about $\lambda = 500$ m for variable T and suggested minimum number of samples N.

T [s]	N	Δf [Hz]	λ_1 [m]	λ_2 [m]	λ_3 [m]
75	128	0.01333	975.8	548.9	351.3
150	256	0.00666	716.9	548.9	433.7
300	512	0.00333	624.5	548.9	486.2
600	1024	0.00166	548.9	516.1	486.2
1200	2048	0.00083	516.1	500.8	486.2
2400	4096	0.00042	508.4	500.8	493.4

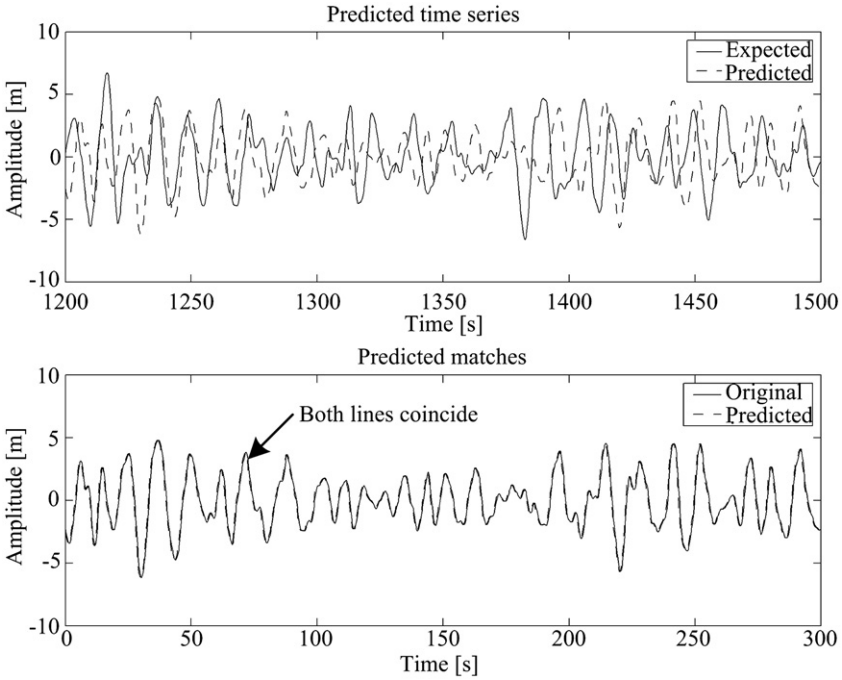

Fig. 2. Predicted time series using Fourier theorem.

appropriate for the time prediction case. Others are working on alternate methods, using the zero-crossing period and amplitude of each wave (looking for a predictable pattern) [40], or through neural networks [21].

4. Prediction in space

The results obtained by other researchers [16,20] using omni-directional spectra (which give good agreement up to 70 m) suggest it would be useful to test just how far ahead (in terms of distance) this prediction method holds.

4.1. Simulation

A reference sensor was positioned at 0 m. Wave records of length 1200 s and 4096 samples were generated for this sensor and at six other positions at distances 50 m, 100 m, 200 m, 300 m, 500 m and 1 km. A 12 m/s Pierson-Moskowitz spectrum, with a range of 0–0.5 Hz and with 256 vectors, was used as the input. The same process of taking the FFT of the record for each position was implemented to generate a sinusoidal series. A different formulation of (1) was used because there were difficulties in obtaining the correct phase angles from the FFT routine used. This new equation is:

$$\zeta(x,t) = \sum_{n=1}^{N/2} a_n \cos(k_n x - \omega_n t) + b_n \sin(k_n x - \omega_n t) \quad (2)$$

where

$$a_n = 2\mathrm{Re}\{\overline{F}_n\} \quad (3)$$

and

$$b_n = -2\mathrm{Im}\{\overline{F}_n\} \quad (4)$$

$\overline{F}_n$ is the raw complex number set returned by the FFT routine; (2) was implemented to obtain a prediction at each sensor. The prediction used $t = \Delta t \rightarrow T$ so that the issue of temporal periodicity did not arise. However x was selected to be at increasing intervals in the target records.

4.2. Results

Fig. 3 shows the results for the 200 m case where a reasonable level of agreement can be seen but with some divergence. The first 300 s period only is displayed here for clarity. The initial 100–150 s of the prediction appears to be worse than the following 150 to 300 s period. Fig. 4 displays the absolute error between the target record and the prediction for the full 1200 s simulation. The higher error level for the first 150 s can be seen with the errors falling to a relatively constant level for the remainder of the record.

Figs. 5 and 6 show the absolute error plots at 100 m and 300 m. A similar pattern to Fig. 4 can be seen where there is a large transient error at the beginning of the prediction which exponentially decreases to a steady background error. This transient is due to

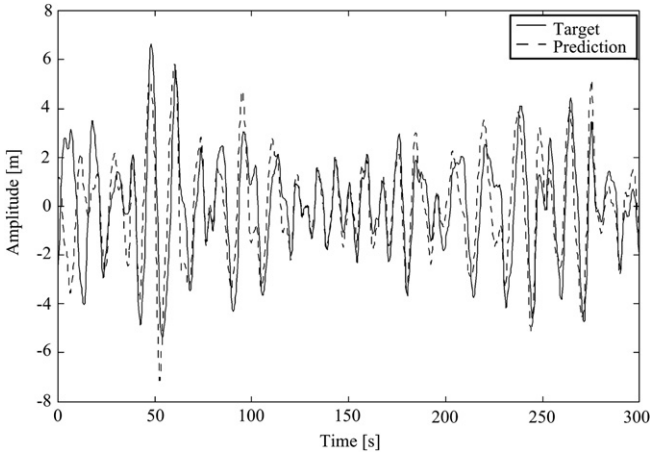

Fig. 3. Prediction made to 200 m.

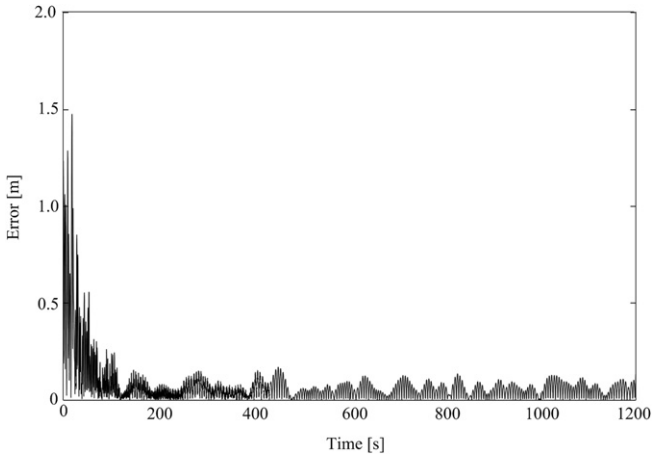

Fig. 4. Absolute errors in prediction made to 200 m.

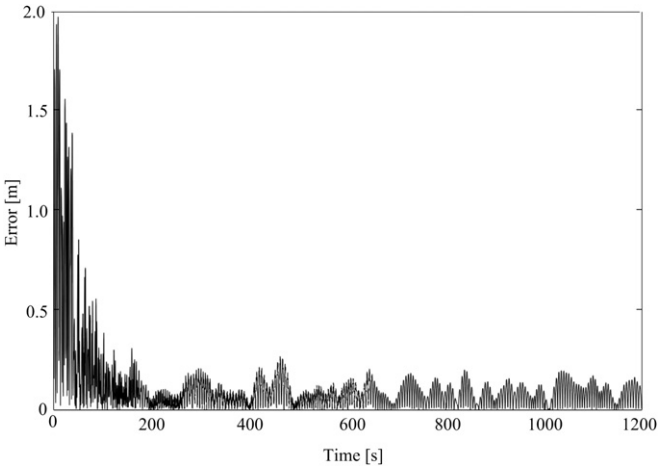

Fig. 6. Absolute errors in prediction made to 300 m.

a prediction being made for the energy which has not yet reached the target sensor. As the energy passes the reference sensor it is recorded as a fluctuation in surface elevation. This energy is travelling at finite velocity and will hence take a certain time to flow from one point to another. The velocity at which energy in a mixed sea state travels is the group velocity. Lower frequency energy moves faster, therefore the time it takes for the highest frequency energy to move to the target sensor determines the time from which a prediction will be valid. Table 2 gives valid-from-times for the six sensor positions used here with an upper frequency bound of 0.5 Hz. The exponentially-decreasing nature of the error is due to the low-frequency high-energy waves reaching the sensor; these build up as the higher frequency waves arrive. In Figs. 4–6, at distances close to the reference sensor, the predictions are reasonably accurate (with residual errors of the order of 0.1 m for the 100 m case). At 200 m and 300 m the errors begin to increase. For simplicity, the complete time series comparisons are omitted; however, it is found that at greater distances, the prediction error levels increase to the point were peaks occur when there should be toughs.

So far only a single wind speed of 12 m/s has been used. The simulations were repeated for wind speeds in the range of 6–30 m/s. The absolute error at each time interval was calculated and averaged over the length of the record. This was used with the corresponding significant wave height to give an average percentage error for each wind speed/prediction point combination (illustrated in Fig. 7). Comparison of the returned error values and the corresponding time series show an absolute error value of less than 10% with few peak/trough discrepancies.

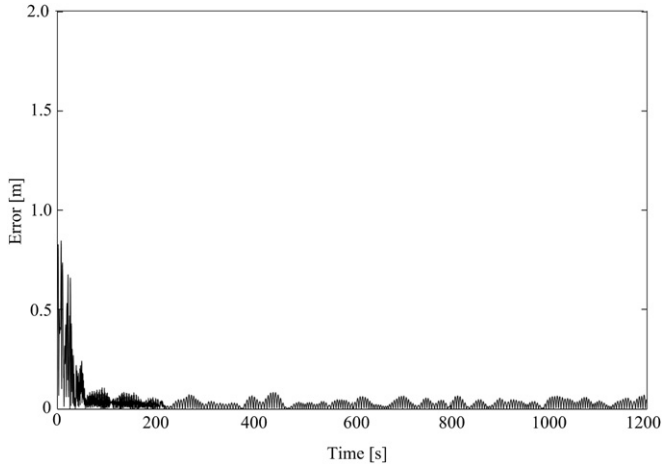

Fig. 5. Absolute errors in prediction made to 100 m.

4.3. Combining temporal and spatial predictions

The two Fourier methods, presented in sections 4.1 and 4.2, for predicting wave records over distance and time can be combined for the case of predicting 50 m ahead and 30 s into the future. This is shown in Fig. 8.

Following on from earlier experiments the results obtained were as expected. The initial 30s of the record in Fig. 8, 1170 s–1200 s correspond to a prediction over distance of 50 m and show a good match. Extending the record beyond 1200 s results in a divergence from the target result.

5. Discussion

The results from the simulations in Section 4 where taken in conjunction with Fig. 7 show that a prediction made to 200 m can be considered valid for a wind speed of less than 16 m/s. This would appear to confirm the findings of [18], [19] and [20]. At distances greater than 200 m the predictions degrade with increasing wind speed. The anomaly of the 1000 m prediction is assumed to be a peculiarity in taking the absolute error between the target and the prediction. It should level out at 50–60% for high wind speed. This is an observation based on the results here and inferred from previous studies.

The prediction degradation with distance and wind speed can be attributed to three factors: (a) the dispersion relationship; (b) the manner in which energy is transported and (c) how we choose to represent this in discrete time and space.

Table 2
Valid-from prediction times.

Sensor distance [m]	Valid-from times [s]
50	32
100	64
200	128
300	192
500	320
1000	641

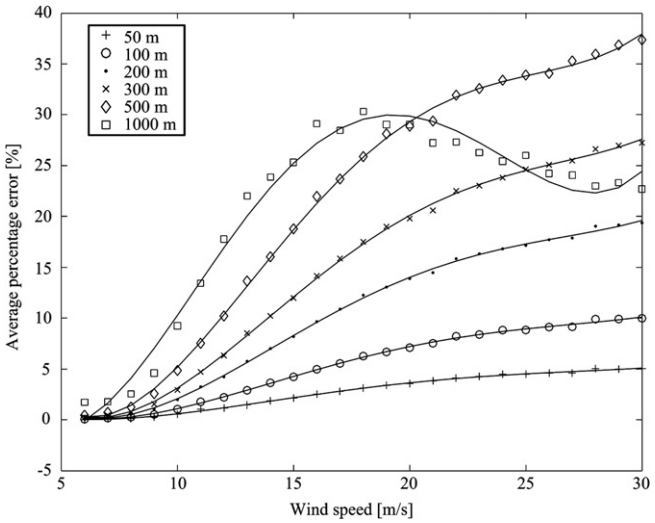

Fig. 7. Average percentage errors with wind speed and distance.

5.1. Discretization of a continuous spectrum

The most straightforward way to examine the manner in which wave energy is represented is to look at the spectrum from which the wave vector files were created. This is related to the manner in which the wave vectors are derived from the FFT of the reference time series. The most common method of representing a mixed wave field is to create a plot of the energy density spectrum. This is the most concise manner in which to represent the data. With the creation of wave vector files and the FFT, the continuous spectrum is effectively sliced into strips of energy of width Δf. These represent a discretely located sinusoid with an amplitude proportional to the energy bounded by $S(f)$ and Δf where

$$a(n\Delta f) = \sqrt{S(n\Delta f)2\Delta f} \tag{5}$$

Fig. 9 shows this process with a 16 m/s Pierson-Moskowitz spectrum where the energy is represented by a sinusoid at 0.125 Hz. With $\Delta f = 0.005$ Hz, this delta function represents the continuous energy over the range 0.1225 Hz–0.1275 Hz.

Using (1), an idealized wave vector (Fig. 9) can be easily propagated, but only if all the energy in the band taken from the original

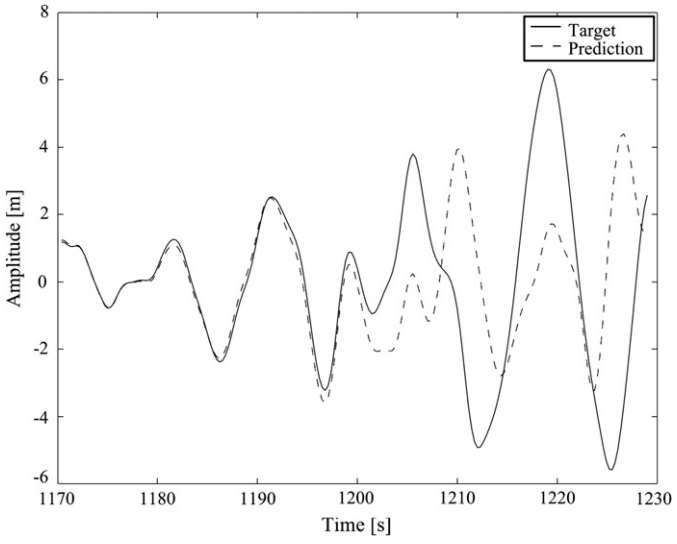

Fig. 8. Prediction for 50 m and 30 s into the future.

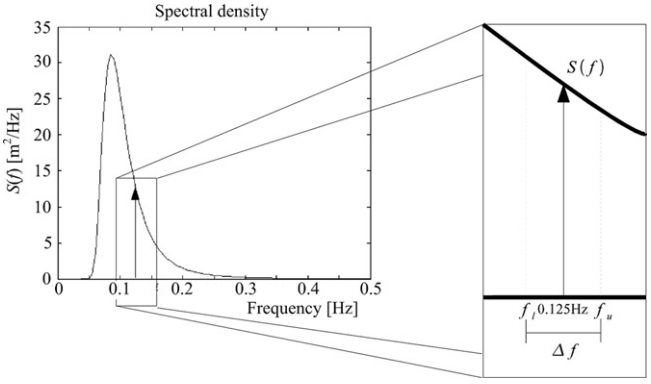

Fig. 9. Discrete representation of continuous energy spectrum.

spectrum can be exactly represented by a single wave vector. In the case of real waves this will never be the case. The energy is spread continuously over the band. From the modelling assumption above, the delta function at 0.125 Hz is taken to represent the range from 0.1225 Hz to 0.1275 Hz. Restating in terms of wavelength (Table 1), a 99.8 m wave represents the range from 95.9 m to 103.9 m. The difference is 8 m which, in terms of cumulative wave vector, can change a trough to a peak.

The dispersion relationship is also important; a wave of longer wavelength will travel faster. For Δf, the energy at the lower frequency will tend to overtake the energy at the higher frequency. This was highlighted in Section 4.2.

5.2. Energy representation

Further simulations can show how the energy in specific bands can be represented. This leads to vastly varying effects on the surface displacement whilst still retaining the original energy. To model the situation, Δf can be modelled by an infinite number of idealized wave vectors; as long as the sum of the energy equals the energy in Δf. To do this Δf has to be split into two bands: 0.12375 Hz and 0.12625 Hz for 0.125 Hz. The amplitudes are proportional to the newly subdivided energy bands. Squaring and summing these amplitudes gives the same energy present in the original band Δf. The process can be continued indefinitely. Table 3 shows the first four levels of subdivision, the energy in each sub-band and the summations of these energies (which are equal to the original). Simulating each of these representations for 1200 s and the taking the FFT of each result gives the same general spectral shape and magnitude. However, if the time series are compared the differences between each becomes

Table 3
Different representations of an energy band.

Δf [Hz]	f [Hz]	Wavelength [m]	Amplitude [m]	Energy = Σ(amplitude)^2
0.005	0.125	99.9238	0.3528	0.1246
0.0025	0.12375	101.9526	0.1118	0.1246
	0.12625	97.9549	0.0821	
0.00125	0.123125	102.9903	0.0629	0.1246
	0.124375	100.9306	0.0497	
	0.125625	98.9320	0.0402	
	0.126875	96.9922	0.0333	
0.000625	0.122812	103.5151	0.0629	0.1246
	0.123437	102.4695	0.0497	
	0.124062	101.4397	0.0402	
	0.124687	100.4253	0.0333	
	0.125312	99.4260	0.0629	
	0.125937	98.4416	0.0497	
	0.126562	97.4718	0.0402	
	0.127187	96.5162	0.0333	

apparent. Fig. 10 shows the 0.125 Hz energy band represented as 1, 2, 4 and 8 discrete wave vectors. In the second graph beating between two closely spaced frequencies is seen. The usual method of explaining the lower two time series is to proceed with a description of group velocity.

When the representation of the energy is repeatedly broken down into finer gradations it is unlikely to produce a more accurate representation of the continuous spectrum. Firstly, no matter how small the band is taken, it can be divided into infinitely smaller vectors and the time representation at one gradation will not generally correspond to those for finer vectors. Fig. 10 illustrates this to a level of 4 orders smaller. It is presumed that if line 10 of Table 3 is taken (a wave vector of frequency 0.124062 Hz), and broken down into finer representations of the same energy, they will not reconstruct to give the same original time series.

A further problem occurs in that the energy banding imposed on the spectrum is for purely mathematical purposes and the wave vectors in the band centred on 0.125 Hz will interact with the frequencies above and below. The classical explanation of group velocity with two frequencies is too simple to apply to the continuous case.

5.3. Relationship to predicted results

The theory of discrete representation can be related to the results in Fig. 7. The errors increase with distance and wind speed. With increasing wind speed, the peak of the spectrum, and hence the concentration of energy, moves to lower frequencies. At the lower frequencies the FFT has decreased resolution, as shown in Table 1. This resolution can only be increased by taking a longer T and hence contracting Δf. The length of T is ultimately governed by the degree of stationarity required for the FFT to remain valid. For longer T there is more of a chance that the sea state and the energy content is going to change.

The increase in error with distance can be explained by the energy contained within Δf. There is more time for the energy to disperse before the prediction point is reached. At short distances the delay between the low-frequency energy and the high frequency energy arriving will be small and the reconstructed energy band should be similar to the original. At greater distances there will be more time for the energy in the band to disperse so that the reconstruction will become more inaccurate.

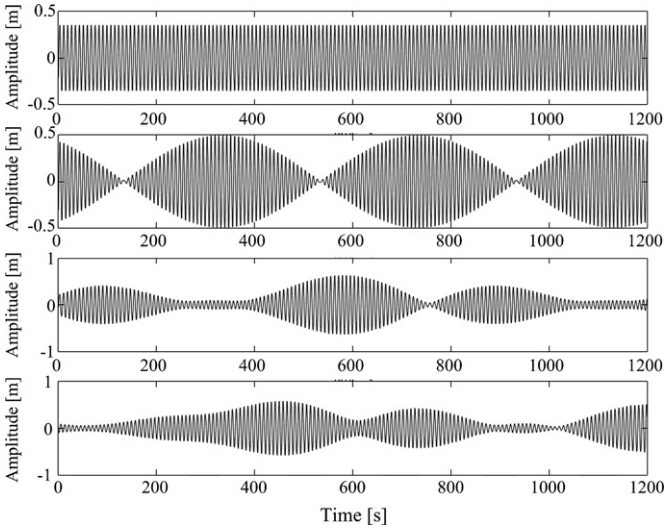

Fig. 10. Prediction for 50 m and 30 s into the future.

6. Conclusions

This paper has explored the use of the FFT in making predictions of wave elevation. The inherent discrete properties of the FFT have not been found to be adequate to deal with the dispersal nature of complex sea waves even where directional influence is not considered. In terms of prediction in time, the periodic nature of the FFT does not fit comfortably with the continuous non-periodic signal it is being fed with. Extending the wave vectors, which are derived from the Fourier components, results in a repetition of the series from which the components came.

Predicting over distance, while working well over short distances, has been shown to be complicated by the different velocities at which the energy within a frequency band travels. The simulations reported in the literature, and the simulations presented here, succeeded in generating predictions over distance. However they were only tested within a restricted wave-tank environment or with simulated data. Further work is needed to test these modelling techniques when subjected to real wave measurements.

In real sea conditions a swell sea and local sea will exist simultaneously, causing further complications to the FFT. Zhang's method [17] would appear to cover this situation using the FFT. Closer examination of the WAve Modelling Group (WAM) [41] and Simulating WAves Nearshore (SWAN) [42] models in conjunction with the FFT methodology presented here may also provide for further avenues of investigation. At present the WAM and SWAN models operate on much larger time and dimensional scales than are appropriate for the short-term problem, but the physics and computational routines on which they are based may prove useful.

References

[1] Iglesias G, López M, Carballo R, Castro A, Fraguela JA, Frigaard P. Wave energy potential in Galicia (NW Spain). Renewable Energy Nov 2009;34(11):2323–33.
[2] Defne Z, Haas KA, Fritz HM. Wave power potential along the Atlantic coast of the southeastern USA. Renewable Energy Oct 2009;34(10):2197–205.
[3] Rusu E, Guedes Soares C. Numerical modelling to estimate the spatial distribution of the wave energy in the Portuguese nearshore. Renewable Energy June 2009;34(6):1501–16.
[4] Dunnett D, Wallace JS. Electricity generation from wave power in Canada. Renewable Energy Jan 2009;34(1):179–95.
[5] Palha A, Mendes L, Juana Fortes C, Brito-Melo A, Sarmento A. The impact of wave energy farms in the shoreline wave climate: Portuguese pilot zone case study using Pelamis energy wave devices. Renewable Energy Jan 2010;35(1):62–77.
[6] Folley M, Whittaker TJT. Analysis of the nearshore wave energy resource. Renewable Energy July 2009;34(7):1709–15.
[7] Nobre A, Pacheco M, Jorge R, Lopes MFP, Gato LMC. Geo-spatial multi-criteria analysis for wave energy conversion system deployment. Renewable Energy Jan 2009;34(1):97–111.
[8] Faizal M, Rafiuddin Ahmeda M, Lee Young-Ho. On utilizing the orbital motion in water waves to drive a Savonius rotor. Renewable Energy Jan 2010;35(1):164–9.
[9] Elwood D, Yim SC, Prudell J, Stillinger C, von Jouanne A, Brekken T, et al. Design, construction, and ocean testing of a taut-moored dual-body wave energy converter with a linear generator power take-off. Renewable Energy Feb 2010;35(2):348–54.
[10] Paixão Conde JM, Gato LMC. Numerical study of the air-flow in an oscillating water column wave energy converter. Renewable Energy Dec 2008;33(12):2637–44.
[11] Jayashankar V, Anand S, Geetha T, Santhakumar S, Jagadeesh Kumar V, Ravindran M, et al. A twin unidirectional impulse turbine topology for OWC based wave energy plants. Renewable Energy March 2009;34(3):692–8.
[12] Halliday JR, Dorrell DG and Wood A. Fourier Approach to Short Term Deterministic Wave Prediction. The Sixteenth (2006) International Offshore and Polar Engineering Conference. San Francisco (California, USA). ISOPE-2006, May 28–June 2, 2006.
[13] WaveNet. Results from the work of the European Thematic Network on Wave Energy. European Community, Report No. ERK5-CT-1999–20001, 2000–2003.
[14] Falnes J. Ocean waves and oscillating systems. ISBN. Cambridge University Press, ISBN 0-521-01749-1; 2002.
[15] Salter SH, Taylor JRM and Caldwell NJ. Power conversion mechanisms for wave energy. Proceedings of the Institute of Mechanical Engineers, 216, Part M, 2002. p 1–27.
[16] Belmont MR, Morris EL, Zienkiewicz HK. Short term forecasting of the sea surface shape. Journal of International Shipbuilding Progress 1998;45(444):383–400.

[17] Zhang J, Yang J, Wen J, Preslin I, Hong K. Deterministic wave model for short-crested ocean waves: Part I. Theory and numerical scheme. Applied Ocean Research 1999;21:167–88.
[18] Pizer DJ, Retzler C, Henderson R, Cowieson MFL, Shaw MG, Dickens B and Hart R. Pelamis WEC- recent advances in the numerical and experimental modeling programme. 6th European Wave and Tidal Energy Conference. Glasgow (UK). 30 Aug – 2 Sept, 2005.
[19] Skourup J and Sterndorff MJ. Deterministic reproduction of nonlinear waves. Proceedings of OMAE'02. Oslo (Norway). June 2002. p. 23–28.
[20] Voronovich V, Holmes B and Thomas G. A preliminary numerical and experimental study of wave prediction. 6th European Wave and Tidal Energy Conference. UK. 30 Aug - 2 Sept, 2005.
[21] Tsai C-P, Lin C, Shen J-N. Neural network for wave forecasting among multi-stations. Ocean Engineering Oct 2002;29(13):1683–95.
[22] Pinto JP, Bernardino MC, Pires Silva A. A Kalman filter application to a spectral wave model. Nonlinear Processes in Geophysics 2005;12:775–82.
[23] Hwang PA, Huang NE, Wang DW. A note on analyzing nonlinear and nonstationary ocean wave data. Applied Ocean Research 2003;25:187–93.
[24] Stopa JE, Cheung KF, Chen Y-L. Assessment of wave energy resources in Hawaii. Journal on Renewable Energy Feb 2011;36(2):554–67.
[25] Boronowski S, Wild P, Rowe A, Cornelis van Kooten G. Integration of wave power in Haida Gwaii. Journal on Renewable Energy Nov 2010;35(11):2415–21.
[26] Abbaspour M, Rahimi R. Iran atlas of offshore renewable energies. Journal on Renewable Energy Jan 2011;36(1):388–98.
[27] Iglesias G, Carballo R. Wave energy and nearshore hot spots: the case of the SE Bay of Biscay. Journal on Renewable Energy Nov 2010;35(11):2490–500.
[28] Palha A, Mendes L, Juana Fortes C, Brito-Melo A, Sarmento A. The impact of wave energy farms in the shoreline wave climate: Portuguese pilot zone case study using Pelamis energy wave devices. Journal on Renewable Energy Jan 2010;35(1):62–77.
[29] Beatty SJ, Wild P, Buckham BJ. Integration of a wave energy converter into the electricity supply of a remote Alaskan island. Journal on Renewable Energy June 2010;35(6):1203–13.
[30] Dolores Esteban M, Javier Diez J, López JS, Negro V. Why offshore wind energy? Journal on Renewable Energy Feb 2011;36(2):444–50.
[31] Amundarain M, Alberdi M, Garrido AJ, Garrido I, Maseda J. Wave energy plants: control strategies for avoiding the stalling behaviour in the Wells turbine. Journal on Renewable Energy Dec 2010;35(12):2639–48.
[32] Workhorse Monitor ADCP User's Guide, RD Instruments, P/N 957-6165-00, USA, January 2001.
[33] Belmont MR, Horwood JMK, Thurley RWF and Baker J. Hallow Angle Wave Profiling LIDAR. 9th IEEE/OES Working Conference on Current Measurement Technology CMTC. March 2008. p. 17–19
[34] Tucker MJ, Pitt EG. Waves in Ocean Engineering. ISBN. Elsevier, ISBN 0-08-043566-1; 2001.
[35] Krogstad HE, Barstow SF, Aasen SE, Rodriguez I. Some recent developments in wave buoy measurement technology. Coastal Engineering 1999;37:309–29.
[36] Allender J, Audunson T, Barstow SF, Bjerken S, Krogstad HE, Steinbakke P, et al. The WADIC project: a comprehensive field evaluation of directional wave instrumentation. Journal of Ocean Engineering 1989;16(5/6):505–36.
[37] Wang HT, Freise CB. Error analysis of the directional wave spectra obtained by the NDBC 3-m Pitch-roll Discus buoy. IEEE Journal of Oceanic Engineering Oct 1997;22(4):639–48.
[38] Dean RG, Dalrymple RA. Water wave mechanics for scientists and engineers. ISBN. World Scientific, ISBN 9-81020-421-3; 1991.
[39] Yemm RW. "The history and status of the Pelamis wave energy converter", wave power: Moving towards Commercial Viability. IMechE, ISBN 1-86058-305-9; 2000.
[40] Stansell P, Wolframb J, Zacharyc S. Horizontal asymmetry and steepness distributions for wind-driven ocean waves from severe storms. Applied Ocean Research June 2003;25(3):137–55.
[41] Komen GJ, Calvaleri L, Donelan M, Hasselmann K, Hasselmann S, Janssen PAE,M. Dynamics and modelling of Ocean waves. Cambridge University Press, ISBN 0-521-57781-0; 1994.
[42] Booij N, Ris C, Holthuijsen LH. A third-generation wave model for coastal regions. Journal of Geophysical Research 1999;104(C4):7649–66.